ACS APPLIED MATERIALS & INTERFACES

Research Article

www.acsami.org

Newly Elaborated Multipurpose Polymer Electrolyte Encompassing RTILs for Smart Energy-Efficient Devices

Jijeesh R. Nair,* Luca Porcarelli, Federico Bella, and Claudio Gerbaldi*

GAME Lab, CHENERGY Group, Department of Applied Science and Technology (DISAT), Politecnico di Torino, Corso Duca degli Abruzzi 24, 10129 Torino, Italy

Supporting Information

ABSTRACT: Profoundly ion-conducting, self-standing, and tack-free ethylene oxide-based polymer electrolytes encompassing a room-temperature ionic liquid (RTIL) with specific amounts of lithium salt are successfully prepared via a rapid and easily upscalable process including a UV irradiation step. All prepared materials are thoroughly characterized in terms of their physical, chemical, and morphological properties and eventually galvanostatically cycled in lab-scale lithium batteries (LIBs) exploiting a novel direct polymerization procedure to get intimate electrode/electrolyte interfacial characteristics. The promising multipurpose characteristics of the newly elaborated materials are demonstrated by testing them in dye-sensitized solar cells (DSSCs), where the introduction of the iodine/iodide-based redox mediator in the polymer matrix assured the functioning of a lab-scale test cell with conversion efficiency exceeding 6% at 1 sun. The reported results enlighten the promising prospects of the material to be successfully implemented as stable, durable, and efficient electrolyte in next-generation energy conversion and storage devices.

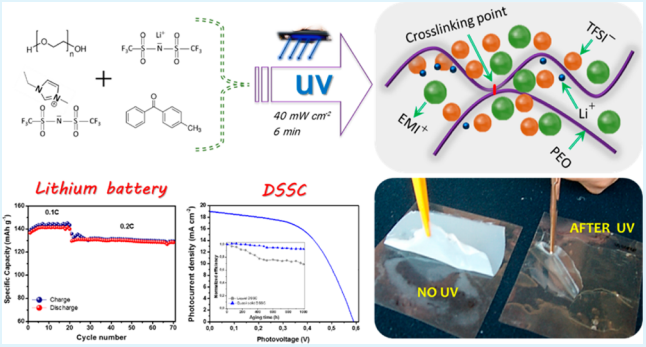

KEYWORDS: *polymer electrolyte, photopolymerization, ionic liquid, lithium battery, dye-sensitized solar cell, multipurpose materials*

1. INTRODUCTION

Wide interest is mounting in the field of polymer electrolytes, due to their application in energy-efficient devices such as rechargeable batteries,[1,2] photoelectrochemical cells,[3,4] electrochromic devices,[5,6] fuel cells,[7,8] and supercapacitors.[9,10] Many of these technologies have already achieved high-level performance that would be expendable at the market level, but some necessary requisites must be fulfilled, especially in terms of safety, mechanical robustness, and durability.[11,12] To meet these demands, quasi- and/or truly solid polymer electrolytes (SPEs) have been recently developed, and it is widely accepted by the scientific community that such materials may allow these technologies to smoothly transfer from the academic to the industrial level.[13−15] Indeed, polymer electrolytes exhibit unique advantages such as mechanical integrity, a wide variety of fabrication methods in desirable size and shape, and the possibility to fabricate an intimate electrode/electrolyte interface and adapt to a lightweight and economic packaging structure. They also guarantee remarkable safety features as no volatile liquids are present and/or if present can appropriately be retained in the polymer matrix. Thus, the usual consequences such as leaking of the liquid electrolyte and related hazards may be eventually avoided.[16,17]

Many polymers (especially those polar) are able to dissolve salts and form complexes, but not all guarantee sufficient ionic mobility due to strong intermolecular forces.[18] Poly(vinylidene fluoride) (PVDF) and its copolymer poly(vinylidenefluoride-*co*-hexafluoropropylene) (P(VDF-*co*-HFP)),[19] polyvinyl chloride (PVC), polyacrylonitrile (PAN), poly(methyl methacrylate) (PMMA), etc., have been widely studied as polymer matrices either in the form of gels or as solid films.[20,21] In the case of PVDF and its copolymers,[22] solvents must be used to convert them in the form of a thin film. Moreover, their cost is still a concern. The battery community is moving toward replacing PVDF as binder as well, shifting to more water-based cellulose-derived materials. Since the discovery of ionic conductivity of alkali metal salt complexes in poly(ethylene oxide) (PEO) by Wright in 1973,[23] intensive research efforts have been focused on these systems containing lithium salts to be implemented as electrolyte separators in secondary batteries.[24] However, the very low ambient temperature conductivity ($<10^{-7}$ S cm^{-1}) of PEO still restricts its practical application in highly demanding energy conversion and storage devices, such as dye-sensitized solar cells (DSSCs) and lithium batteries (LIBs). Many attempts have been made to improve the ionic conductivity of PEO, including the introduction of inorganic fillers,[25] the use of specifically designed counterions,[26] the chemical functionalization of its polymeric chains,[27] the design of interpenetrating cross-linked networks,[28] etc. In recent years, room-temperature ionic liquids (RTILs) have been intensively investigated due to

Received: March 29, 2015
Accepted: May 28, 2015
Published: May 28, 2015

DOI: 10.1021/acsami.5b02729
ACS Appl. Mater. Interfaces 2015, 7, 12961−12971

their excellent properties such as very low volatility, nonflammability, high thermal stability, and conductivity up to 1 mS cm^{-1}.[29,30] These factors render RTILs suitable for application in electrochemical systems being highly performing, efficient, safe, and durable.

Another key factor that influences the fate of a polymer electrolyte is the synthetic procedure that enables a facile and rapid large-scale manufacturing process. In this respect, photopolymerization is a low-temperature procedure: upon UV irradiation, a multifunctional monomer gets converted into a cross-linked polymer network by means of a chain reaction induced by reactive species (free radicals) generated by a photoinitiator.[31] Photoinduced polymerization is an ideal preparation method for polymer electrolytes in the electrochemistry field, due to its attractive features, including low energy consumption, absence of solvents and catalysts, rapidity, and low cost.[32] Previously, our group demonstrated innovative ways to adapt the photopolymerization process for the production of polymer electrolytes, especially in the field of Li-ion batteries,[33] dye-sensitized solar cells,[34] and capacitors.[35] Photocured polymer matrices for the energy conversion and storage fields have also been proposed by other groups.[36−38]

In this article, a highly conductive PEO-based polymer electrolyte is prepared via direct free-radical photopolymerization in the presence of a lithium salt and an imidazolium-based RTIL. Sensationally elastomeric, resistant, and self-standing membranes are obtained and characterized in terms of ionic conductivity, electrochemical stability, mechanical properties, thermal and interfacial stability. Generally, RTILs are simply mixed with a thermoplastic polymeric material with or without the presence of additives[39] or they are mixed with various cross-linking agents to improve the overall stability.[33] In the present case, we are demonstrating that without using any solvents and any tiring synthesis steps a softly cross-linked polymer matrix can be elaborated within a few minutes. Significantly, the feasibility of using such material in LiBs at different temperatures was established, also thanks to a suitable in situ polymerization procedure directly on the surface of the electrode films, fundamental to obtain an intimate interfacial adhesion. The process is simple, eco-friendly, and even adaptable to battery-processing methods to achieve better interfaces. Moreover, it is also demonstrated that the polymer membrane can be used to achieve high-efficiency values in DSSCs without drastically changing the components or processes. To the best of our knowledge, this is the first report on the multipurpose characteristics of a UV cross-linked imidazolium-based polymer electrolyte membrane, guaranteeing excellent and durable performances in both energy conversion and storage lab-scale devices. In addition, the simplicity of the proposed process and the wide availability of the materials used make this system very promising and ready to be industrially scaled up following the main principles of green chemistry.

2. EXPERIMENTAL SECTION

2.1. Materials. All starting materials and reagents were purchased from commercial suppliers and used without any further purification. PEO (average $M_v \approx 10^6$, Sigma-Aldrich) was vacuum dried overnight at 50 °C before use. Lithium bis(trifluoromethane sulfonyl) imide salt (LiTFSI, $CF_3SO_2NLiSO_2CF_3$, 99.9% purity, battery grade, Solvionic) and 1-ethyl-3-methylimidazolium-bis(trifluoromethyl-sulfonyl) imide (EMI-TFSI, $C_8H_{11}F_6N_3O_4S_2$, 99.5%, Solvionic) were vacuum dried overnight at 100 °C before use. The free-radical photoinitiator 2-methyl-benzophenone (MBP, $CH_3C_6H_4COC_6H_5$, ≥99%, Sigma-Aldrich) and lithium metal foils (Li, high-purity lithium foils, Chemetall Foote Corp.) were used as received. Lithium iron phosphate ($LiFePO_4$) was supplied by Lithops s.r.l. Sodium iodide (NaI), iodine (I_2), and acetonitrile were purchased from Sigma-Aldrich and used as received. Conducting glass plates (FTO glass, fluorine-doped tin oxide overlayer, sheet resistance 7 Ω sq^{-1}, purchased from Solaronix) were cut into 2 cm × 2 cm sheets and used as substrate for both the deposition of a TiO_2 porous thin layer from a paste (DSL 18NR-AO, Dyesol) and the fabrication of platinized counter electrodes. Sensitizing dye *cis*-diisothiocyanato-bis(2,2′-bipyridyl-4,4′-dicarboxylato)ruthenium(II) bis(tetrabutylammonium) (N719, Ruthenizer 535 bis-TBA) was purchased from Solaronix. All substances were stored in an argon-filled dry glovebox (MBRAUN LABstar) having a humidity content below 1 ppm.

2.2. Preparation of the Polymer Electrolytes. An optimal PEO:EMI-TFSI:LiTFSI polymer electrolyte composition was selected, which is 45:45:10 in weight ratio. Before arriving to the reported formulation, several tests were performed to understand the fundamental aspects of polymer electrolytes to decide the quantity and type of photoinitiator as well as the suitable molecular weight of PEO depending on the easiness in processing, solubility of salt, ionic mobility in terms of [EO]/[Li] ratio, and mechanical integrity. MBP was selected as the photo-cross-linker with superior solubility and optimum cross-linking properties in the 5% w/w ratio with respect to the PEO content. Such studies are not included in the manuscript being out of the aim of the present discussion. The ternary polymer electrolyte was prepared adapting an existent literature protocol first proposed by Rupp et al.[40] Initially, a homogeneous solution of EMI-TFSI, lithium salt, and the photoinitiator was prepared by mixing the components at 50 °C for 1 h. Subsequently, PEO and the latter solution were blended in a mortar to promote homogeneous mixing; the mixture was left at 120 °C for 2 h under inert atmosphere. Then the mixture was sandwiched between two Mylar sheets and reduced into a thin film by a hot press at 90 °C at 50 bar for 15 min. Without removing the Mylar sheets, the film was UV cured for 3 min per side under a xenon arc lamp (Helios Italquartz, 45 mW cm^{-2}). Before any further use, the obtained polymer electrolyte films (thickness of 90 ± 5 μm, measured using Thickness Gages Series 547 equipped with an ABSOLUTE Digimatic Indicator from Mitutoyo) were dried overnight under high vacuum at 45 °C. All above-reported procedures were carried out in an environmentally controlled dry room (10 m^2, RH < 2 ± 1% at 20 °C) manufactured by Soimar.

2.3. Characterization of the Polymer Electrolytes. The insoluble fraction of the UV-cured ternary polymer electrolyte was determined as follows: a typical sample was accurately weighed and, subsequently, extracted in $CHCl_3$ (Sigma-Aldrich) for 18 h to dissolve the non-cross-linked soluble chains. After extraction, the insoluble fraction was dried at 60 °C to ensure the complete removal of the solvent, which guarantees a constant weight. The insoluble fraction was calculated dividing the dry sample weight by the calculated weight of PEO in the starting polymer.

Differential scanning calorimetry (DSC) was performed in the temperature range between −80 and 120 °C at a heating rate of 10 °C min^{-1} under nitrogen atmosphere. For analysis, the sample was first heated up to 120 °C, then rapidly cooled down to −80 °C, and scanned. The DSC traces were recorded with a DSC 204 F1 Phoenix (Netzsch) instrument, equipped with a low-temperature probe. Thermogravimetric analysis (TGA) was carried out under nitrogen atmosphere in the temperature range between 25 and 600 °C with a TG 209 F1 Libra instrument (Netzsch) at a heating rate of 10 °C min^{-1}.

Mechanical measurements on the samples were carried out through tensile experiments according to ASTM Standard D638 using a INSTRON 3366 dynamometer-equipped electromechanical extensimeter (clip gauge) with a load cell of 500N; data were elaborated using the software provided by Instron S.r.l. A constant deformation of 10 mm min^{-1} was applied on strips of 1 cm in width, which were blocked at an initial distance of 2.5 cm. At least five specimens for each sample were tested; the standard deviation in Young modulus (E) was 5%.

DOI: 10.1021/acsami.5b02729
ACS Appl. Mater. Interfaces 2015, 7, 12961−12971

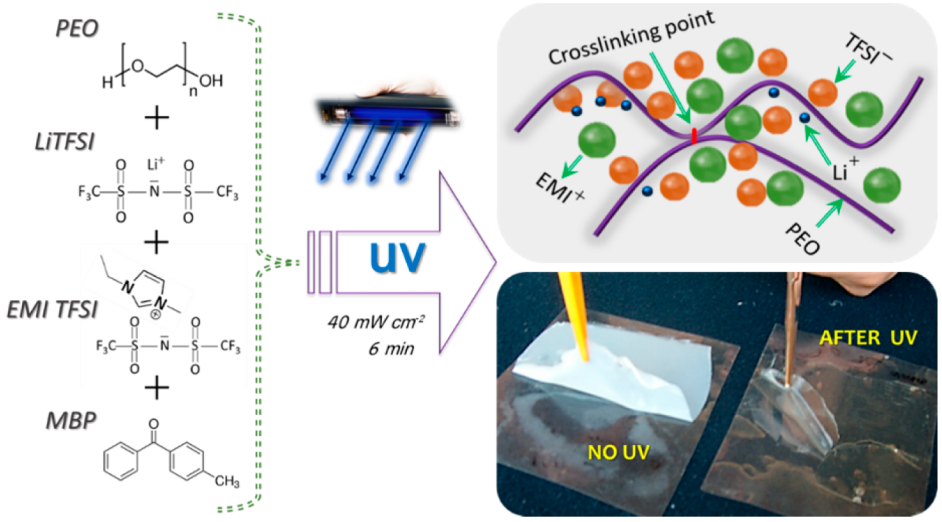

Figure 1. All components used in the study along with the real aspect of the polymer electrolyte formed after UV exposure (on the right bottom side), which is almost transparent, tack free, flexible, and easy to manage. (Right top side) Hypothesized interlinking of polymer chains encompassing imidazolium-based RTIL.

The overall morphology of the prepared samples was investigated by field emission scanning electron microscopy (FESEM, ZEISS Supra 40), equipped with an energy-dispersive X-ray (EDX) spectrometer. For analysis, samples were subjected to metallization by sputtering a very thin Cr layer (around 10 nm maximum) to minimize the charging and burning effect caused by high-energy electron beam irradiation. To perform cross-sectional analysis, samples were cracked under cryogenic conditions after dipping in liquid nitrogen for enough time to avoid any change in the morphology.

Ionic conductivity (σ) was determined by electrochemical impedance spectroscopy (EIS) analysis of cells assembled by sandwiching a disk of the polymer electrolyte between two stainless steel (SS-316) blocking electrodes. The cells were assembled in the dry room and housed in an environmental simulation chamber (BINDER model MK-53, with a temperature control of ±1 °C). A PARSTAT-2273 frequency response analyzer (Princeton Applied Research) was used to measure the cell impedance in the frequency range from 100 kHz to 1 Hz at the open-circuit potential (OCV) between 20 and 80 °C with 10 °C intervals. Test cells were allowed to reach the thermal equilibrium for at least 1 h before each test. The ionic conductivity was calculated based on the equation

$$\sigma = \frac{l}{A}\frac{1}{R_\Omega} \quad (1)$$

where R_Ω is the ohmic resistance of the polymer electrolyte while l and A are the thickness and the area of the polymer electrolyte sample, respectively. R_Ω was obtained from the impedance value at the intercept of the semicircle with the real axis in the low-frequency region of the Nyquist plot. The reproducibility of the obtained results was confirmed with at least three replicates.

The lithium transference number (t_{Li+}) was determined by a dc polarization combined with impedance spectroscopy, as described in Ferrari et al.[41] (see detailed description in the Supporting Information).

The electrochemical stability window was evaluated by cyclic voltammetry at ambient temperature with a CHI600 electrochemical analyzer/workstation (CH Instruments). Measurements on fresh samples were performed to separately evaluate the anodic stability window (ASW) and the cathodic stability window (CSW). To measure the ASW, an electrochemical test cell with a lithium metal reference electrode model ECC-ref (EL-CELL, Germany) was assembled placing the polymer electrolyte sample between a stainless steel working electrode and a lithium metal disk counter electrode. The cell potential was scanned toward more positive values starting from the OCV to the upper limit of 5.5 V vs Li^+/Li and then scanned back toward the OCV. To measure the CSW, a copper disk-working electrode was used and the cell potential was scanned from the OCV to −0.3 V vs Li^+/Li. The scan rate was fixed at 0.1 mV s^{-1} for both measurements.

2.4. Fabrication and Characterization of LIBs. Laboratory-scale lithium cells were tested in terms of galvanostatic charge/discharge cycling at different current rates with an Arbin Instrument Testing System model BT-2000. Potential cut offs are given in section 3. Cell assembly was performed inside the dry glovebox. A two-electrode electrochemical test cell model ECC-Std (EL-CELL) was assembled using a $LiFePO_4$-based composite working electrode and a lithium metal counter electrode. The $LiFePO_4$-based composite electrode was prepared by casting and successively drying a 1-methyl-2-pyrrolidone (NMP, Sigma-Aldrich) slurry having the composition 88:6:6 w/w in $LiFePO_4$ (active material, Clariant LP2), electronic conductivity enhancer AB50 (Shawinigan Black AB50, Chevron Corp.), and binder PVdF (Solvay Solef 6020). The electrodes were vacuum dried for 5 h at 120 °C before use.

The cell was assembled by combining a lithium metal anode with an electrode−electrolyte composite prepared by light curing the polymer electrolyte directly onto the $LiFePO_4$ cathode film surface. In a typical preparation, a blend of UV-cured polymer electrolyte was prepared following the procedure described in section 2.2 and placed between the electrode and a Mylar sheet. The mixture was reduced into a film by hot pressing and followed up with a light-induced photopolymerization directly over the electrode.[42] Then electrolyte/electrode disks (area 2.54 cm^2) were cut from the sheet and dried under vacuum overnight at 55 °C prior to cell assembly.

2.5. Fabrication and Characterization of DSSCs. Photoanode preparation started by washing FTO-covered glasses with acetone and ethanol in an ultrasonic bath for 10 min. Then all traces of solvents were removed by flash evaporation on a hot plate at 450 °C. The DSL 18NR-AO active opaque titania paste was deposited onto FTO by doctor-blade technique and successively dried at 100 °C for 10 min on a hot plate. A sintering process at 525 °C for 30 min allowed the formation of a nanoporous TiO_2 layer having an average thickness of 8 ± 0.3 μm, measured by a profilometer (P.10 KLA-Tencor Profiler). The sensitization of the photoelectrodes was performed by soaking to a 0.4 mM N719 dye solution in ethanol overnight at ambient temperature, followed by washing in ethanol to remove the unadsorbed dye. On the other hand, counter electrodes consisted of FTO-glass platinized slices prepared by depositing a 5 nm thick Pt thin film by thermal evaporation.

The photocured polymer electrolyte membranes were activated by swelling in a liquid electrolyte composed of NaI and I_2 (a 10:1 molar

DOI: 10.1021/acsami.5b02729
ACS Appl. Mater. Interfaces 2015, 7, 12961−12971

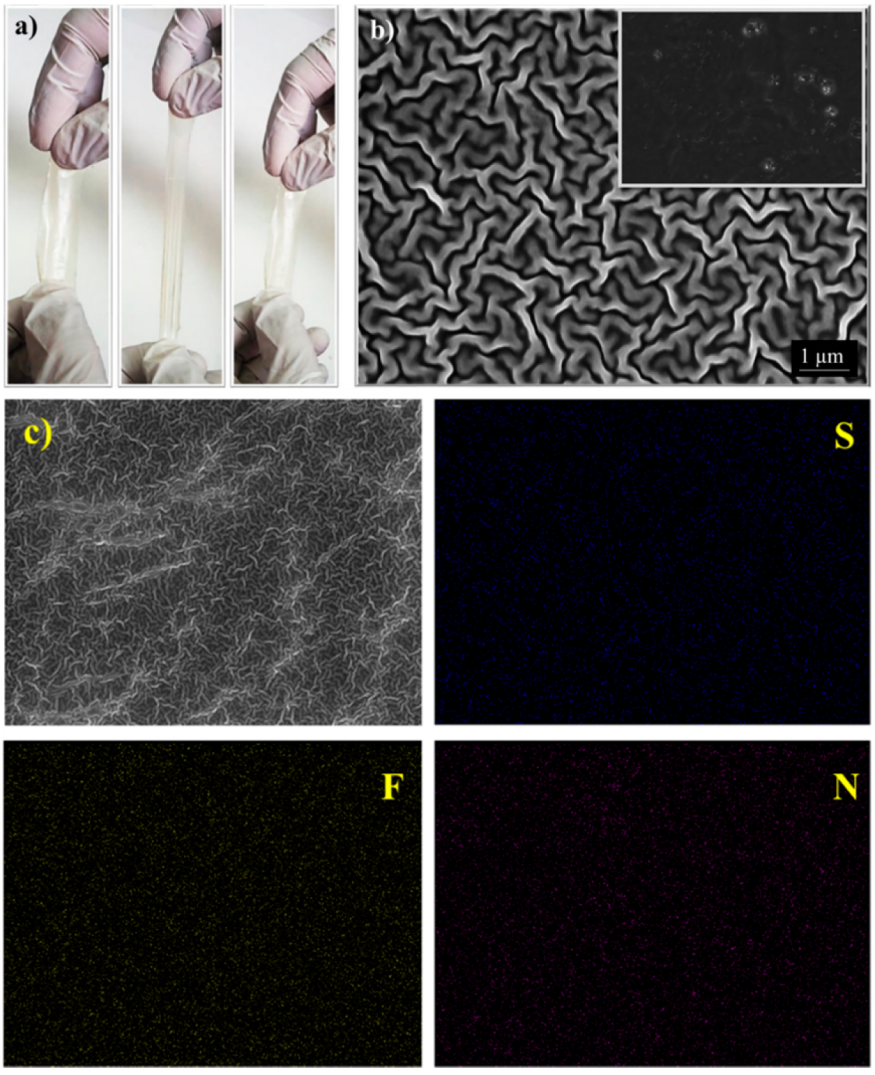

Figure 2. (a) Appearance of the light-cured cross-linked polymer electrolyte sample upon manual elongation, (b) FESEM analysis at high magnification of the sample surface, (c) focus on the area (30 μm × 30 μm) of the image where EDX analysis was carried out, along with the following images in which S, F, and N indicate the distribution of sulfur, fluorine, and nitrogen, respectively, of $TFSI^-$ anion in the selected area of the sample.

ratio was chosen) dissolved in acetonitrile. Polymeric electrolyte membranes were sandwiched between photoanodes and cathodes in a sandwich-like architecture. A cyanoacrylate-based glue was used for the final sealing. The photocurrent−photovoltage curves were recorded on an electrochemical station (Lanlike Chemical Electronic High-Tech Ltd.). A solar light simulator (Oriel 91160) was used as the white light source to give AM 1.5G and 100 mW cm^{-2} illumination on the surface of the solar cells with a mask of 0.20 cm^2 aperture. The intensity of the incident light was calibrated with a radiant power/energy meter (Oriel 70260) before each experiment.

3. RESULTS AND DISCUSSION

3.1. Characterization of the Polymer Electrolytes. The precursor mixture comprising PEO, RTIL, LiTFSI, and the hydrogen abstraction photoinitiator (MBP), after hot pressing and UV light exposure, formed a transparent, self-standing, and nontacky polymer electrolyte membrane, as shown in Figure 1. Under UV excitation, MBP abstracts a proton from a methylene group and generates a free radical on the PEO chain.[40] This free radical can combine with another free radical from the same chain or a neighbor chain and create a cross-linking point (see also the sketched picture of Figure 1). Polymer electrolytes composed of PEO and Li salts typically use [EO]/[Li] mole ratio as a parameter to increase the mobile Li cation content; in our selected formulation, an [EO] to [Li] ratio of 30:1 was considered as optimal.

The mechanical robustness of the cross-linked polymer electrolyte is shown in Figure 2a, where the remarkable elasticity is demonstrated. It is impressive to note that the sample is easily stretchable and highly flexible, as demonstrated by the ability to retain its original shape and size after the stress is released.

FESEM analysis was conducted to characterize the morphology of the photocured polymer films. A representative top view is shown in Figure 2b; the surface of the cross-linked polymer presents a uniform wrinkled texture, resulting from the fabrication method adopted. The bright and dark areas in the image belong to amorphous PEO domains alternated to some residual ordered (semicrystalline) domains, respectively; the wrinkled texture derives from the formation of cross-linking domains between the polymer chains. Similar kinds of textures are also present in polymer films kept at a certain temperature under high stress (50 bar for 15 min at 90 °C) during the

DOI: 10.1021/acsami.5b02729
ACS Appl. Mater. Interfaces 2015, 7, 12961−12971

preparation process. Once the stress is removed the chain may tend to come back to its normal state (stress release), but the subsequent cross-linking process and related heat induced by the UV light help the matrix to freeze to its shape in wrinkled form. In systems such as thin films, it is observed that wrinkles may form up on heating, which is initiated by a thermomechanical instability, and the resulting pattern evolution is termed spinodal wrinkling.[43] The dispersion force[44,45] and a higher temperature (flow temperature), which is superior than the T_g during processing, will play a vital role to determine the type, style, and dimensions of wrinkles.[46] In our case, the surface morphology appears to be highly regular, thus confirming a good blending between the components of the ternary mixture. A similar precursor mixture processed without a UV irradiation step generated a nonuniform and hardly homogeneous membrane (inset of Figure 2b). On the contrary, the cross-linking produced by UV irradiation allows the incorporation of the same amount of RTIL and salt, leading to a material with dramatically different morphological characteristics in terms of homogeneity and robustness. Moreover, the UV-cured PEO-based network is able to efficiently hold the RTIL without any leakage. Furthermore, the EDX analysis shown in Figure 2c further confirmed the homogeneous distribution of S, N, and F elements present in the $TFSI^-$ anion, which is an indirect indication that the prepared polymer electrolyte is highly homogeneous.

Gel content studies guaranteed that the UV irradiation on the sample for overall 6 min was sufficient to form a well-cross-linked film with high reproducibility. Indeed, the insoluble fraction of the samples was found to be higher than 95% with respect to the total PEO content after 18 h of extraction in $CHCl_3$. This confirms that all PEO chains incorporated in the polymer matrix were in the cross-linked form.

Mechanical properties were evaluated by tensile analysis; typical force (N)−elongation (mm) curves for both UV-irradiated and nonirradiated samples are shown in Figure 3.

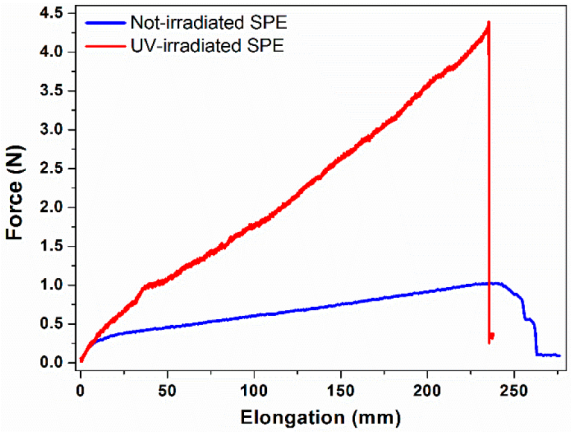

Figure 3. Mechanical measurements carried out on UV-irradiated and nonirradiated SPEs at ambient temperature by traction test.

They reveal that the average Young's modulus E of the SPE before UV irradiation (0.4 ± 0.05 MPa) is higher than the SPE after UV irradiation (0.2 ± 0.05 MPa). Nevertheless, contrary to what normally is observed, the UV-irradiated SPE showed higher tensile resistance R_{max} (1.45 ± 0.05 MPa) than the nonirradiated SPE (0.6 ± 0.15 MPa). It can be also drawn from Figure 3 that the overall area under the stress/strain curve of UV-irradiated SPE is much higher than the one not exposed to UV light, which makes the material tougher. Such a tough behavior is highly demanding in materials conceived for flexible applications. If one considers that there is 45 wt % of ionic liquid incorporated, these are highly satisfying values.

The results of the thermogravimetric study are shown in Figure 4a. As a reference, all components of the SPE were tested separately. EMI-TFSI is thermally stable up to 450 °C and shows a one-step degradation process. PEO and LiTFSI decompose at slightly lower temperature (around 400 °C), again with a well-defined single-step process. The resulting cross-linked polymer electrolyte shows a two-step weight loss process: the first one, occurring at around 400 °C, corresponds to the decomposition of the PEO matrix and embedded lithium salt. The second step corresponds to EMI-TFSI degradation and occurs around 450 °C. The first dip before reaching 100 °C is ascribed to the loss of humidity that may be absorbed during the handling of the sample for testing. Overall, we can claim a thermal stability up to 375 °C under inert conditions, and such a remarkable result is particularly interesting for application in LIBs and DSSCs with increased safety.

The plasticizing effect of EMI-TFSI on the polymer electrolyte was studied by DSC, the results of which are shown in Figure 4b. The glass transition of the polymer electrolyte occurs at −56 °C. Interestingly, the melting of the crystalline phase of PEO is occurring at about 20 °C, viz. much lower temperature than the standard PEO melting. The shift may occur due to several reasons, such as the addition of lithium salt, addition of EMI-TFSI, and most importantly the cross-linking reaction, which only allow restricted movement of the −EO− chains to reorganize themselves to form crystallites. Even though the interlinking between the chains is not uniform, the crystallites formed by the reactions could be smaller, which may reflect the lowering of the melting of crystalline peaks. Moreover, the starting point of the broadening peak could be an indication of just PEO chain rearrangement rather than melting. Another possibility might be the melting of some excess LiTFSI-EMI-TFSI phase as reported by Shin et al.[39] Overall, the degree of crystallinity was effectively minimized to the nearly fully amorphous state by addition of Li salt, RTIL, and the UV-induced cross-linking process.

XRD was used to get further confirmation of the fundamental role of the photocuring step in reducing the overall crystallinity of the PEO-based SPE to nearly fully amorphous state (see Figure 5). Pristine PEO showed intense characteristic peaks corresponding to the crystalline features of the polymer matrix. The addition of EMI-TFSI, LiTFSI, along with the UV-induced photopolymerization process greatly reduced the intensity of the peaks along with almost negligible reflections between 15° and 25° (peaks at 2θ = 37° and 44° are due to the aluminum sample holder), thus indicating an almost completely amorphous polymer electrolyte. Indeed, this is in agreement with the DSC graphs obtained for the same sample.

The ionic conductivity of solid polymer electrolytes at ambient temperature is usually 2−3 orders of magnitude lower than that of a liquid electrolyte, thus precluding their practical application in standard LIBs.[20] It is well known that PEO crystallization reduces ionic conductivity. To overcome this issue, EMI-TFSI was incorporated into the polymer matrix. The ionic conductivity of the polymer electrolyte in the temperature interval between 20 and 80 °C is shown in Figure 6. At 20 °C the σ value is equal to 2.5×10^{-4} S cm^{-1}. This result is of particular interest as it is sufficiently high to allow ambient-

DOI: 10.1021/acsami.5b02729
ACS Appl. Mater. Interfaces 2015, 7, 12961−12971

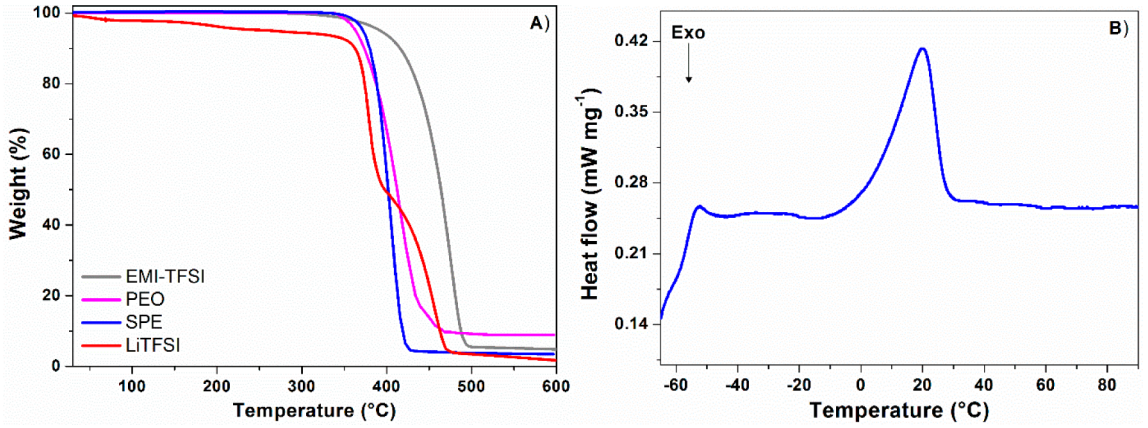

Figure 4. Thermal characteristics of the materials: (a) TGA profiles and (b) DSC trace.

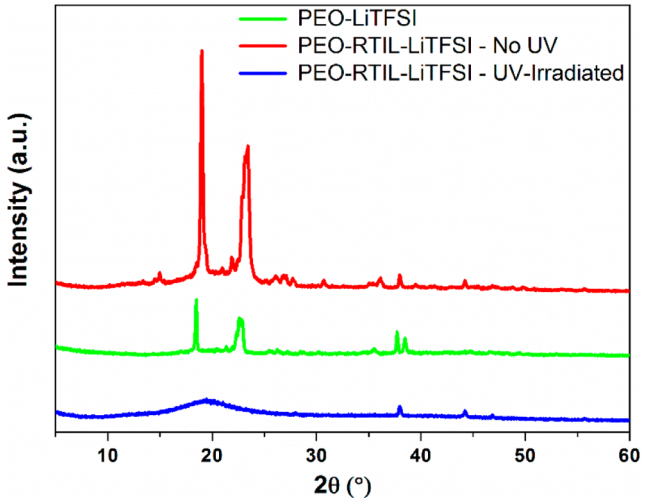

Figure 5. X-ray diffraction (XRD) analysis of the different samples.

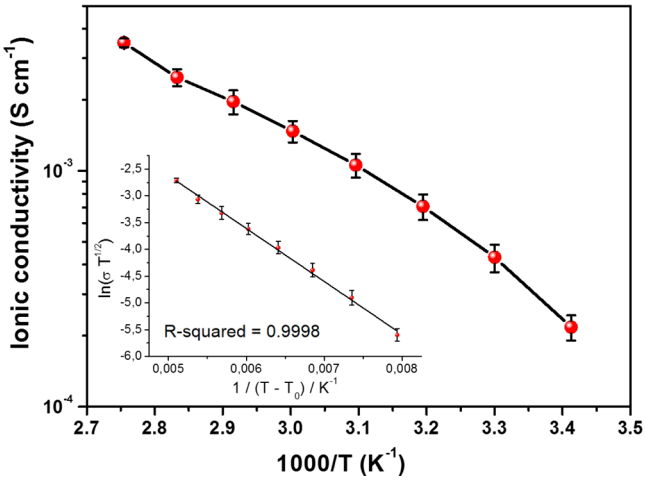

Figure 6. Arrhenius plot for ionic conductivity as a function of temperature of the polymer electrolyte membrane (inset, fitting by means of the VTF equation). Data obtained by impedance spectroscopy.

temperature operation of Li-ion cells. It exceeds 10^{-3} S cm^{-1} already at 50 °C. The Vogel−Tamman−Fulcher (VTF)[47−49] behavior of the SPE was verified fitting the conductivity data with respect to temperature. The *R*-square value confirms the quality of the fitting. The value of the activation energy was found to be 8.23 kJ mol^{-1}. This result is in good accordance with the DSC study discussed in the previous paragraph. Beneficial effects coming from the incorporation of EMI-TFSI in the polymer matrix were observed, including its plasticizing effect, which reduces the crystalline degree of PEO and provides a high-mobility phase for Li^+ ions to be transported through the SPE.[50] Despite increasing the ionic conductivity, the incorporation of ionic liquids usually leads to loss of mechanical stability. The UV cross-linking process allows preparing stable polymer electrolyte having both high ionic conductivity and excellent mechanical properties. Although a different mixture of PEO, lithium salts, and RTILs has been proposed in recent years, the RT conductivity herein presented is of particular interest since it matches values obtained with a higher amount of lithium salts or even exceeds values obtained with a higher amount of RTIL.[51]

An appropriate assessment of the ionic conduction in polymer electrolytes and its influence on the other electrochemical properties can be derived from lithium-ion transport behavior. The lithium transference number, t_{Li+}, is a key factor in the optimization of electrolytes encompassing RTIL and Li salt for Li and Li-ion battery; in fact, high t_{Li+} guarantees high power density. As typically observed when using polymer electrolyte systems encompassing RTIL and salts,[41] t_{Li+} of the polymer electrolyte membrane was found not to be very high (note that the calculated mole ratio of Li^+/EMI^+ in our proposed system equals 0.3:1). It resulted in 0.165 at 55 °C, which is in good agreement with recent literature reports.[41,52]

3.2. Evaluation of the Performances in All-Solid Lithium Polymer Cell. A secondary lithium-based battery typically operates between 0.02 and 4.2 V vs Li^+/Li; therefore, the ESW of the electrolyte must be wider than the operating potential in order to ensure high Coulombic efficiencies and long stable cycling. The electrochemical stability limits of the polymer electrolyte were evaluated by cyclic voltammetry, and the results are shown in Figure 7. Despite a shoulder centered at 4.2 V vs Li^+/Li being clearly visible in the CV, the main anodic breakdown potential of the polymer occurs at above 4.6 V vs Li^+/Li, as indicated by a steep increase in the anodic current exceeding the current threshold of 0.01 mA cm^{-2}. This is also supported by a literature finding for similar systems encompassing EMI-based RTILs.[53,54] Above this potential, the electrolyte starts to decompose by oxidative irreversible reactions. Upon cathodic scan toward more negative potential values, a small cathodic current that does not exceed the

DOI: 10.1021/acsami.5b02729
ACS Appl. Mater. Interfaces 2015, 7, 12961−12971

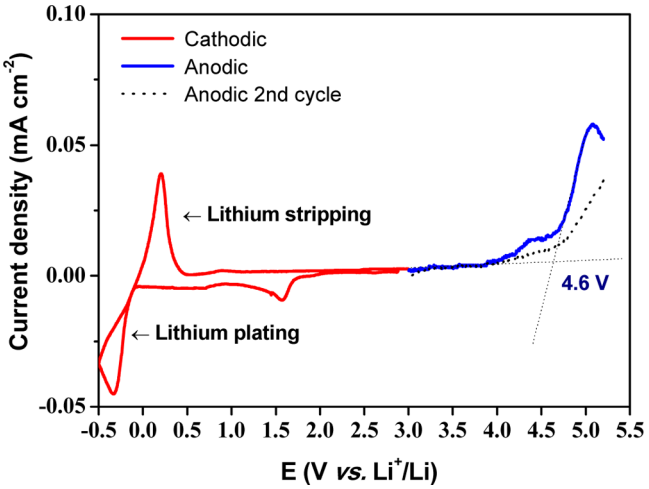

Figure 7. Electrochemical stability window (ESW) of the polymer electrolyte at ambient temperature; potential scan rate of 0.1 mV s^{-1}.

current threshold is observed; this event is most likely associated with reduction of the electron deficient C2 carbon of the imidazolium ring;[54] the multistep decomposition of some impurity traces in EMI-TFSI (used as received) may not be excluded. However, this phenomenon is neglectable due to the solid character of the electrolyte. The interpretations on both anodic and cathodic behaviors are supported by the following findings: (i) the irreversibility of the peaks, and (ii) the trend of the second sweep cycle where the gradual disappearance of the events is detected (e.g., the 4.2 V shoulder peak in the second anodic scan). An overall good cathodic electrochemical stability is indicated by the lithium plating/stripping, which is clearly evident at around 0 V vs Li^+/Li. The most important information that can be assumed from the ESW test are as follows: (i) the presence of a well-defined lithium deposition/stripping couple of peaks confirms both the proper working of the solid polymer electrolyte in lithium cell as well as the presence of a porous and ion-transporting interface, (ii) the safe operation of the system under standard working conditions, since the anodic breakdown occurs at potentials higher than 4 V versus Li, and (iii) the purity of the entire system demonstrated by the very flat plateau in the stability region.[55]

In view of practical applications, the polymer electrolyte membrane was assembled in a lab-scale all-solid-state lithium polymer cell, and its electrochemical behavior was investigated by means of galvanostatic charge/discharge cycling as a function of the cycle number at ambient temperature. The cell was assembled by combining a lithium metal anode with an electrode−electrolyte composite prepared by light curing the polymer electrolyte directly onto the $LiFePO_4$ cathode surface, a rapid and easily scalable procedure detailed in section 2.4. One major drawback related to the use of solid polymer electrolytes is the unsufficient contact between the active materials of the electrode and the polymer matrix. The hot-press step we adopted, instead, was fundamental to obtain a good penetration of the polymer electrolyte precursor into the composite cathode. In fact, the melted PEO/RTIL blend is likely to fill the porosity of the electrode, thus ensuring good wetting of the active material particles. A very thin (~30 μm thickness) and mechanically robust polymer electrolyte film with excellent adhesion to the electrode surface was then obtained after the subsequent direct photopolymerization procedure. Moreover, the cross-linked polymer matrix is able to effectively retain the RTIL; thus, no leakage is guaranteed (confirmed by conductivity measurements in which the bulk resistance of the electrolyte was stable after several thermal cycles as well as 15 days of storage at 55 °C). FESEM images taken after cracking the sample are given in Figure 8. In particular, at higher magnifications, it can be clearly observed that the electrolyte layer creates a conformal coating by following the contours of the electrode particles. This results in improved active area at the interface between the electrode and the polymer electrolyte, correspondingly reflected in improved specific energy and specific power of the cell.[56] The oriented cross-linked polymer electrolyte morphology is clearly evident on top of the electrode along with the optimum interface and interpenetration between the electrode active material particles and the electrolyte.

The response of the cell is shown in Figure 9. Constant current charge/discharge profiles extracted from cycling tests carried out at increasing cycling rates at mild temperature (55 °C) are shown in plot A of Figure 9. They reflect the good properties of the newly elaborated system, showing definite flat potential plateaus both on charge and on discharge related to the typical biphasic Li^+ extraction/insertion mechanism in

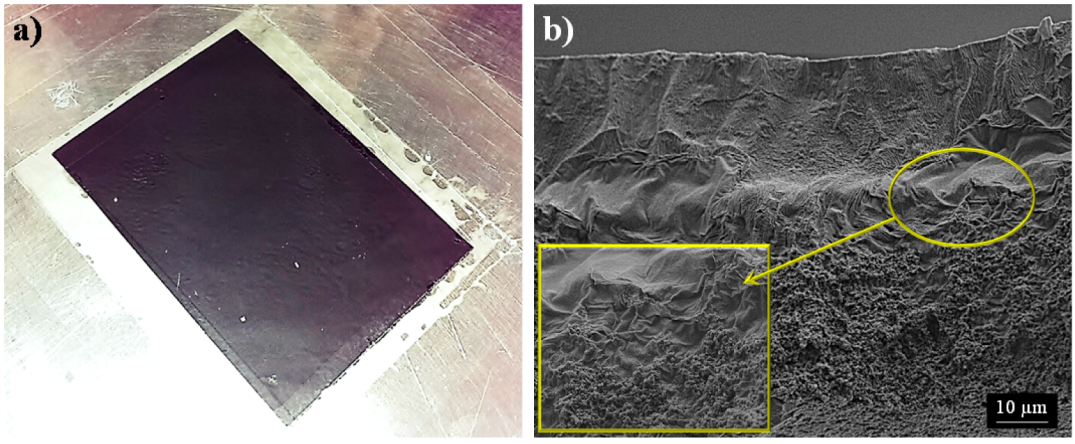

Figure 8. (a) Photograph of a freshly prepared self-supporting multiphase electrode/electrolyte composite obtained by direct hot pressing and in situ photopolymerization of the polymer electrolyte on top of the $LiFePO_4$ composite electrode. (b) Cross-sectional FESEM images illustrating the morphology of the multiphase electrode/electrolyte composite at different degree of magnification.

DOI: 10.1021/acsami.5b02729
ACS Appl. Mater. Interfaces 2015, 7, 12961−12971

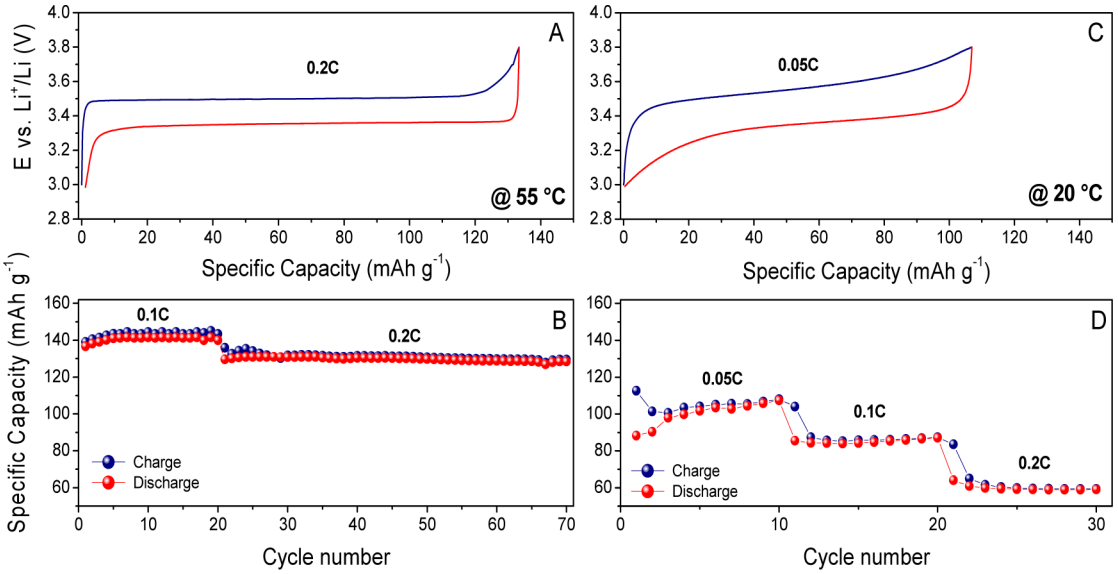

Figure 9. Cycling behavior of the solid polymer lithium cell assembled by contacting the $LiFePO_4$-based electrode/polymer electrolyte with a lithium metal anode in the 3.0−3.8 V vs Li^+/Li range at different temperatures: (a) constant current charge/discharge potential vs specific capacity profiles extracted from cycle 70 at 0.2 C rate, (b) specific capacity vs cycle number plot at different C rates at 55 °C, (c) constant current charge/discharge potential vs specific capacity profiles extracted from cycle 10 at 0.05 C rate, and (d) specific capacity vs cycle number plot at different C rates at 20 °C.

$LiFePO_4$, well in agreement with the characteristics of the selected active material: at about 3.5 V vs Li^+/Li upon charge (i.e., Li^+ deinsertion from the $LiFePO_4$ structure) and at about 3.35 V vs Li^+/Li upon discharge (i.e., Li^+ insertion into the $FePO_4$ structure), with a steep potential increase/decay at its end.[57] The polarization was found to be very limited even at 0.2 C rate. This fact accounts for efficient redox reaction kinetics, due to both limited internal resistance at the electrode/electrolyte interface and limited cell overpotential contributions. In general, the material shows a good cycling stability at each of the tested current regimes, as for the good overlapping of the charge/discharge curves, accounting for a charge coefficient (charge capacity/following discharge capacity) very close to unity.

The maximum specific capacity values obtained by the $LiFePO_4$/electrolyte composite developed in this work (see plot B of Figure 9) are about 143 and 132 mAh g^{-1} at 0.1 and 0.2 C, respectively. Noteworthy, the newly developed polymer electrolyte demonstrated the ability to be reversibly cycled at 20 °C as well (again exploiting the direct in situ polymerization, see plots C and D in Figure 9), still retaining stable response at each current density. Note that the same commercial $LiFePO_4$ material tested in the same cell assembled in our laboratories using a standard liquid electrolyte can provide about 157 and 145 mAh g^{-1} at the same current regimes. Overall, although the specific capacity obtained is slightly lower than that obtained for the same $LiFePO_4$ cathode material at the same currents in liquid electrolyte, the polymer cell showed good capacity retention exceeding 91%. This is a convincing indication of a good interfacial contact between the electrodes and the electrolyte separator, arising from the fabrication procedure adopted. Nevertheless, full specific capacity was not obtained, even at low current regime, which indicates that we were not able to get the full wetting of the active material surface; such an issue might be solved by optimizing the polymer electrolyte formulation and fabrication procedure or even developing three-dimensional porous solid electrolyte with high surface area, thus allowing the increase of the interface region. The rate capability of the lithium metal polymer cell was also excellent. Good performance at high current rate may be ascribed to the efficient ionic conduction in the polymer-coated separator and the favorable interfacial charge transport between the electrodes and the electrolyte in the cell. The sum of these phenomena along with the simple, fast, and ecofriendly preparation procedure allow one to realize the optimum conditions for the newly elaborated material to act as solid polymer electrolyte in LIBs.

3.3. Evaluation of the Performance in Quasi-Solid DSSCs. The photocured polymer electrolytes encompassing RTIL were activated by proper swelling in a liquid electrolyte composed of NaI and I_2 (a 10:1 molar ratio was chosen) dissolved in acetonitrile. This step allowed the redox mediator to enter and remain in the void spaces within the 3D-cross-linked network. The obtained quasi-solid polymer electrolytes were still free-standing and nontacky, although extremely flexible and easy to handle. Thus, quasi-solid state DSSCs were assembled by placing each polymer electrolyte membrane onto the N719-sensitized photoanode. After cells sealing with Pt-coated counter electrodes, the photovoltaic parameters were measured under 1 sun irradiation.

In addition to checking the applicability of the polymer electrolyte presented in this work for DSSC application, a careful investigation of the effect of the redox mediator concentration was conducted. Indeed, the iodide concentration is a variable not easily treated, as it affects in the opposite direction the values of photocurrent and photovoltage of the resulting DSSC.[58,59] In previous works on liquid devices,[60] the effect of increasing the iodide concentration positively affected both the photocurrent and the ionic conductivity values: the overall performance increase was attributed to the availability of more iodide ions useful for dye cations regeneration. On the other hand, it was also observed that the increase of the iodide concentration worsened the cell photovoltage, namely, the difference between the Fermi level of TiO_2 (E_F) and the redox

DOI: 10.1021/acsami.5b02729
ACS Appl. Mater. Interfaces 2015, 7, 12961−12971

potential of electrolyte (E), which can be expressed by the Nernst equation

$$E = E^{\circ} - \frac{RT}{NF} \ln \frac{a_R}{a_O} \quad (2)$$

where E° is the standard electrode potential, R is the gas constant, T is the absolute temperature, N is the electron number per one reaction species, F is the Faraday constant, and a_R and a_O are the activities of reduction and oxidation species, respectively.[61] From eq 2 it is easy to notice that the increase of concentration of reducing species (iodide) causes a shift of the redox potential to more negative values. As a consequence, V_{oc} decreases because the energy gap between E_F and E becomes smaller. In summary, it is necessary to find a compromise to obtain the highest possible photocurrent value without significantly lowering the photovoltage.

Cells parameters of quasi-solid DSSCs assembled in this work are listed in Table 1, while the corresponding $J-V$ curves

Table 1. Photovoltaic Parameters of DSSCs Assembled with Polymer Electrolytes Containing Different Concentrations of the Redox Mediator

[NaI] (mol L^{-1})	J_{sc} (mA cm^{-2})	V_{oc} (V)	FF	PCE (%)
0.10	12.40	0.57	0.52	3.70
0.20	14.95	0.56	0.53	4.42
0.30	19.00	0.59	0.55	6.10
0.45	17.10	0.57	0.54	5.22
0.60	15.42	0.56	0.52	4.53

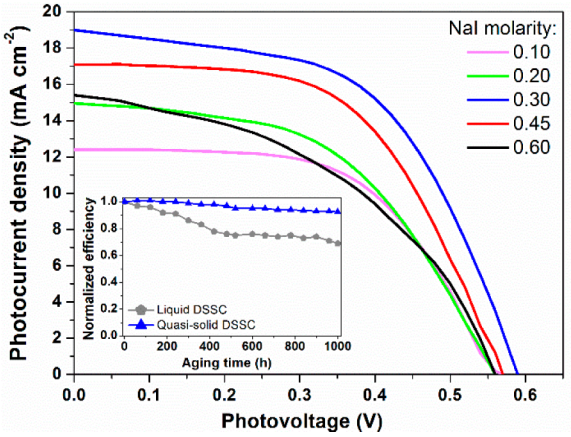

Figure 10. Photocurrent/photovoltage curves of DSSCs assembled with polymer electrolytes containing different concentrations of the redox mediator. (Inset) Normalized PCE for DSSCs assembled with the best polymer electrolyte and the corresponding liquid one vs conservation time under 60 °C.

are plotted in Figure 10. A bell-shaped trend of the cell efficiency as a function of the concentration of NaI in the polymer electrolyte is present. However, contrary to the above-reported literature trends, it is clear that the photovoltage of the quasi-solid cells is not particularly influenced by the variation of the concentration of the redox mediator. On the other hand, the photocurrent grew from 12.40 to 19.00 mA cm^{-2} when the concentration of NaI increased from 0.10 to 0.30 mol L^{-1}. This variation is certainly due to the larger amount of iodide ions that can regenerate the oxidized dye molecules. Then, when the concentration of NaI was further increased to 0.60 mol L^{-1}, the trend was reversed and the photocurrent decreased to 15.42 mA cm^{-2}. The explanation of this phenomenon is certainly the formation of ion pairs in the presence of high NaI concentrations, as it has already been reported for other polymeric systems applied in DSSC devices.[62] Apart from this, it is noteworthy that the maximum efficiency (6.10%) was achieved in the presence of a concentration of NaI equal to 0.30 mol L^{-1}: this value is 40% lower than that usually adopted in the DSSC field. In other words, the polymer electrolyte presented in this work was able to provide excellent performance and avoid the use of high amounts of salts at the same time. The reason for this peculiarity must be sought in the three-dimensional architecture of the photo-cross-linked electrolyte proposed in this work (which favors the ionic motion between cell electrodes) and the capacity of the lithium salts (useful for application in LIBs) to act as supporting electrolytes for the iodine-based redox mediator. Moreover, LiTFSI also acted as lithium-ion (Li^+) donor, the latter able to positively shift of the conduction band of TiO_2.[63] As a result, the electron injection efficiency of the resulting DSSCs was improved, and this was reflected in the high photocurrent values listed in Table 1.

In order to assess the long-term stability of the fabricated DSSCs, a 1000 h aging test was carried out at a temperature of 60 °C in the dark, and the cells were tested every 60 h. The resulting curves, depicted in the inset of Figure 10, show that a reference liquid cell was able to retain less than 70% of its initial efficiency after aging. This finding is consistent with those usually reported in the literature for liquid lab-scale cells[3] and also confirms the tendency of liquid electrolytes not to provide stable long-term performance. In contrast, the polymer electrolyte-based DSSC presented in this work showed only a 7% decay of the initial efficiency, thus demonstrating that the UV-produced polymeric network is able to trap and effectively retain the solvated redox mediator.

4. CONCLUSIONS

In summary, we successfully introduced a novel polymer electrolyte membrane for solid/quasi-solid state energy storage and conversion devices, obtained by a unique, rapid, economic, easily upscalable, and environmentally friendly two-step process including a photocuring step. Compared to other techniques, the production process here proposed appears highly advantageous due to its ease and rapidity in processing. No solvents are employed at any stages of the processing; moreover, the materials used can be eventually recycled, thus making the whole process environmentally benign. This novel fabrication method could reduce the manufacturing cost and simplify the fabrication process.

The new configuration adopted for the production of multiphase electrolyte/electrolyte assembly consisted in the direct formation of the SPE on top of the $LiFePO_4$ composite positive electrode surface by hot pressing followed by UV-induced cross-linking. The characterization and obtained results demonstrated an enhanced adhesion of the polymer electrolyte to the active electrode materials. The lab-scale lithium polymer cell assembled showed stable charge/discharge characteristics without any capacity fading even at 0.2 C current regime. This process plays a critical role in improving the wettability and electrolyte retention, the interfacial adhesion between the electrode active material, and the separator and cycle performance of the resulting lithium polymer cell assembly.

DOI: 10.1021/acsami.5b02729
ACS Appl. Mater. Interfaces 2015, 7, 12961−12971

Due to the intimate contact between the electrode material grains and the polymer electrolyte matrix, the interface does not create problems arising by insufficient contact. Thus, the cell produced by hot pressing combined with light-induced cross-linking holds a great potential to be used in high-performance, versatile, and cost-effective LIBs.

The versatile use of these membranes for other applications such as DSSCs makes this process a strong tool to prepare universal membranes with multipurpose feature. Although further efforts are necessary to reduce the contact resistance, we successfully indicated the adaptability of UV polymerization of PEO to the industrial manufacturing process of all solid state energy production and storage devices.

■ ASSOCIATED CONTENT

Supporting Information

Lithium-ion transference number (t_{Li^+}) study and Nyquist plot of a membrane assembled in a symmetric cell. The Supporting Information is available free of charge on the ACS Publications website at DOI: 10.1021/acsami.5b02729.

■ AUTHOR INFORMATION

Corresponding Authors

*E-mail: jijeesh.nair@polito.it.

*E-mail: claudio.gerbaldi@polito.it.

Notes

The authors declare no competing financial interest.

■ ACKNOWLEDGMENTS

The contribution of Dr. Italo Doberdò is gratefully acknowledged. Lithops batteries S.r.l. is acknowledged for providing the $LiFePO_4$ electrode material. The National University of Malaysia is gratefully acknowledged for the support in photovoltaic measurements.

■ REFERENCES

(1) Croguennec, L.; Palacin, M. R. Recent Achievements on Inorganic Electrode Materials for Lithium-Ion Batteries. *J. Am. Chem. Soc.* **2015**, *137*, 3140−3156.

(2) Kundu, D.; Talaie, E.; Duffort, V.; Nazar, L. F. The Emerging Chemistry of Sodium Ion Batteries for Electrochemical Energy Storage. *Angew. Chem., Int. Ed.* **2015**, *54*, 3432−3448.

(3) Wu, J.; Lan, Z.; Lin, J.; Huang, M.; Huang, Y.; Fan, L.; Luo, G. Electrolytes in Dye-Sensitized Solar Cells. *Chem. Rev.* **2015**, *115*, 2136−2173.

(4) Bella, F. Polymer Electrolytes and Perovskites: Lights and Shadows in Photovoltaic Devices. *Electrochim. Acta* **2015**, DOI: 10.1016/j.electacta.2015.02.195.

(5) Layani, M.; Kamyshny, A.; Magdassi, S. Transparent Conductors Composed of Nanomaterials. *Nanoscale* **2014**, *6*, 5581−5591.

(6) Cannavale, A.; Manca, M.; De Marco, L.; Grisorio, R.; Carallo, S.; Suranna, G. P.; Gigli, G. Photovoltachromic Device with a Micro-patterned Bifunctional Counter Electrode. *ACS Appl. Mater. Interfaces* **2014**, *6*, 2415−2422.

(7) Li, Y.; Wang, S.; He, G.; Wu, H.; Pan, F.; Jiang, Z. Facilitated Transport of Small Molecules and Ions for Energy-Efficient Membranes. *Chem. Soc. Rev.* **2015**, *44*, 103−118.

(8) Sadeghi Alavijeh, A.; Khorasany, R. M. H.; Habisch, A.; Wang, G. G.; Kjeang, E. Creep Properties of Catalyst Coated Membranes for Polymer Electrolyte Fuel Cells. *J. Power Sources* **2015**, *285*, 16−28.

(9) Yu, Z.; Tetard, L.; Zhai, L.; Thomas, J. Supercapacitor Electrode Materials: Nanostructures from 0 to 3 Dimensions. *Energy Environ. Sci.* **2015**, *8*, 702−730.

(10) Staaf, L. G. H.; Lundgren, P.; Enoksson, P. Present and Future Supercapacitor Carbon Electrode Materials for Improved Energy Storage Used in Intelligent Wireless Sensor Systems. *Nano Energy* **2014**, *9*, 128−141.

(11) Amanchukwu, C. V.; Harding, J. R.; Shao-Horn, Y.; Hammond, P. T. Understanding the Chemical Stability of Polymers for Lithium-Air Batteries. *Chem. Mater.* **2015**, *27*, 550−561.

(12) Bella, F.; Griffini, G.; Gerosa, M.; Turri, S.; Bongiovanni, R. Performance and Stability Improvements for Dye-Sensitized Solar Cells in the Presence of Luminescent Coatings. *J. Power Sources* **2015**, *283*, 195−203.

(13) Song, D.; Cho, W.; Lee, J. H.; Kang, Y. S. Toward Higher Energy Conversion Efficiency for Solid Polymer Electrolyte Dye-Sensitized Solar Cells: Ionic conductivity and TiO_2 Pore-Filling. *J. Phys. Chem. Lett.* **2014**, *5*, 1249−1258.

(14) Antolini, E. Iridium as Catalyst and Cocatalyst for Oxygen Evolution/Reduction in Acidic Polymer Electrolyte Membrane Electrolyzers and Fuel Cells. *ACS Catal.* **2014**, *4*, 1426−1440.

(15) Gerbaldi, C.; Nair, J. R.; Kulandainathan, M. A.; Kumar, R. S.; Ferrara, C.; Mustarelli, P.; Stephan, A. M. Innovative High Performing Metal Organic Framework (MOF)-Laden Nanocomposite Polymer Electrolytes for All-Solid-State Lithium Batteries. *J. Mater. Chem. A* **2014**, *2*, 9948−9954.

(16) Hu, P.; Duan, Y.; Hu, D.; Qin, B.; Zhang, J.; Wang, Q.; Liu, Z.; Cui, G.; Chen, L. Rigid-Flexible Coupling High Ionic Conductivity Polymer Electrolyte for an Enhanced Performance of $LiMn_2O_4$/Graphite Battery at Elevated Temperature. *ACS Appl. Mater. Interfaces* **2015**, *7*, 4720−4727.

(17) Shen, S. Y.; Dong, R. X.; Shih, P. T.; Ramamurthy, V.; Lin, J. J.; Ho, K. C. Novel Polymer Gel Electrolyte with Organic Solvents for Quasi-Solid-State Dye-Sensitized Solar Cells. *ACS Appl. Mater. Interfaces* **2014**, *6*, 18489−18496.

(18) Christie, A. M.; Lilley, S. J.; Staunton, E.; Andreev, Y. G.; Bruce, P. G. Increasing the Conductivity of Crystalline Polymer Electrolytes. *Nature* **2005**, *433*, 50−53.

(19) Zhu, Y. S.; Wang, F. X.; Liu, L. L.; Xiao, S. Y.; Chang, Z.; Wu, Y. P. Composite of a Nonwoven Fabric with Poly(Vinylidene Fluoride) as a Gel Membrane of High Safety for Lithium Ion Battery. *Energy Environ. Sci.* **2013**, *6*, 618−624.

(20) Stephan, A. M. Review on Gel Polymer Electrolytes for Lithium Batteries. *Eur. Polym. J.* **2006**, *42*, 21−42.

(21) Mathew, C. M.; Kesavan, K.; Rajendran, S. Dielectric and Thermal Response of Poly[(Vinylidene Chloride)-co-Acrylonitrile]/Poly(Methyl Methacrylate) Blend Membranes. *Polym. Int.* **2015**, *64*, 750−757.

(22) Zhu, Y.; Xiao, S.; Shi, Y.; Yang, Y.; Hou, Y.; Wu, Y. A Composite Gel Polymer Electrolyte with High Performance Based on Poly-(Vinylidene Fluoride) and Polyborate for Lithium Ion Batteries. *Adv. Energy Mater.* **2014**, *4*, No. 1300647.

(23) Fenton, D. E.; Parker, J. M.; Wright, P. V. Complexes of Alkali Metal Ions with Poly(Ethylene Oxide). *Polymer* **1973**, *14*, 589.

(24) Jo, G.; Jeon, H.; Park, M. J. Synthesis of Polymer Electrolytes Based on Poly(Ethylene Oxide) and an Anion-Stabilizing Hard Polymer for Enhancing Conductivity and Cation Transport. *ACS Macro Lett.* **2015**, *4*, 225−230.

(25) Dkhissi, Y.; Huang, F.; Cheng, Y. B.; Caruso, R. A. Quasi-Solid-State Dye-Sensitized Solar Cells on Plastic Substrates. *J. Phys. Chem. C* **2014**, *118*, 16366−16374.

(26) Onishi, K.; Sewa, S.; Asaka, K.; Fujiwara, N.; Oguro, K. The Effects of Counter Ions on Characterization and Performance of a Solid Polymer Electrolyte Actuator. *Electrochim. Acta* **2001**, *46*, 1233−1241.

(27) Rolland, J.; Brassinne, J.; Bourgeois, J. P.; Poggi, E.; Vlad, A.; Gohy, J. F. Chemically Anchored Liquid-PEO Based Block Copolymer Electrolytes for Solid-State Lithium-Ion Batteries. *J. Mater. Chem. A* **2014**, *2*, 11839−11846.

(28) Kuo, P. L.; Wu, C. A.; Lu, C. Y.; Tsao, C. H.; Hsu, C. H.; Hou, S. S. High Performance of Transferring Lithium ion for Polyacrylonitrile-Interpenetrating Crosslinked Polyoxyethylene Network as Gel Polymer Electrolyte. *ACS Appl. Mater. Interfaces* **2014**, *6*, 3156−3162.

(29) Zhang, S.; Sun, J.; Zhang, X.; Xin, J.; Miao, Q.; Wang, J. Ionic Liquid-Based Green Processes for Energy Production. *Chem. Soc. Rev.* **2014**, *43*, 7838−7869.
(30) Macfarlane, D. R.; Tachikawa, N.; Forsyth, M.; Pringle, J. M.; Howlett, P. C.; Elliott, G. D.; Davis, J. H.; Watanabe, M.; Simon, P.; Angell, C. A. Energy Applications of Ionic Liquids. *Energy Environ. Sci.* **2014**, *7*, 232−250.
(31) Crivello, J. V.; Reichmanis, E. Photopolymer Materials and Processes for Advanced Technologies. *Chem. Mater.* **2014**, *26*, 533−548.
(32) Shao, J.; Huang, Y.; Fan, Q. Visible Light Initiating Systems for Photopolymerization: Status, Development and Challenges. *Polym. Chem.* **2014**, *5*, 4195−4210.
(33) Gerbaldi, C.; Nair, J. R.; Ferrari, S.; Chiappone, A.; Meligrana, G.; Zanarini, S.; Mustarelli, P.; Penazzi, N.; Bongiovanni, R. New Electrolyte Membranes for Li-based Cells: Methacrylic Polymers Encompassing Pyrrolidinium-Based Ionic Liquid by Single Step Photopolymerisation. *J. Membr. Sci.* **2012**, *423*−*424*, 459−467.
(34) Sacco, A.; Bella, F.; DeLaPierre, S.; Castellino, M.; Bianco, S.; Bongiovanni, R.; Pirri, C. F. Electrodes/Electrolyte Interfaces in the Presence of a Surface-Modified Photopolymer Electrolyte: Application in Dye-Sensitized Solar Cells. *ChemPhysChem* **2015**, *16*, 960−969.
(35) Ijeri, V. S.; Nair, J. R.; Gerbaldi, C.; Bongiovanni, R. M.; Penazzi, N. Metallopolymer Capacitor in "One Pot" by Self-Directed UV-Assisted Process. *ACS Appl. Mater. Interfaces* **2010**, *2*, 3192−3200.
(36) Wetjen, M.; Kim, G. T.; Joost, M.; Appetecchi, G. B.; Winter, M.; Passerini, S. Thermal and Electrochemical Properties of PEO-LiTFSI-Pyr$_{14}$TFSI-Based Composite Cathodes, Incorporating 4 V-Class Cathode Active Materials. *J. Power Sources* **2014**, *246*, 846−857.
(37) Osada, I.; Von Zamory, J.; Paillard, E.; Passerini, S. Improved Lithium-Metal/Vanadium Pentoxide Polymer Battery Incorporating Crosslinked Ternary Polymer Electrolyte with N-Butyl-N-Methylpyrrolidinium Bis(Perfluoromethanesulfonyl)Imide. *J. Power Sources* **2014**, *271*, 334−341.
(38) Winther-Jensen, O.; Armel, V.; Forsyth, M.; MacFarlane, D. R. In Situ Photopolymerization of a Gel Ionic Liquid Electrolyte in the Presence of Iodine and its Use in Dye Sensitized Solar Cells. *Macromol. Rapid Commun.* **2010**, *31*, 479−483.
(39) Shin, J. H.; Henderson, W. A.; Passerini, S. Ionic Liquids to the Rescue? Overcoming the Ionic Conductivity Limitations of Polymer Electrolytes. *Electrochem. Commun.* **2003**, *5*, 1016−1020.
(40) Rupp, B.; Schmuck, M.; Balducci, A.; Winter, M.; Kern, W. Polymer Electrolyte for Lithium Batteries Based on Photochemically Crosslinked Poly(Ethylene Oxide) and Ionic Liquid. *Eur. Polym. J.* **2008**, *44*, 2986−2990.
(41) Ferrari, S.; Quartarone, E.; Mustarelli, P.; Magistris, A.; Fagnoni, M.; Protti, S.; Gerbaldi, C.; Spinella, A. Lithium ion conducting PVdF-HFP composite gel electrolytes based on N-methoxyethyl-N-methylpyrrolidinium bis(trifluoro-methanesulfonyl)-imide ionic liquid. *J. Power Sources* **2010**, *195*, 559−566.
(42) Gerbaldi, C.; Destro, M.; Nair, J. R.; Ferrari, S.; Quinzeni, I.; Quartarone, E. High-Rate V_2O_5-based Li-Ion Thin Film Polymer Cell with Outstanding Long-Term Cyclability. *Nano Energy* **2013**, *2*, 1279−1286.
(43) Yoo, P. J.; Lee, H. H. Evolution of a Stress-Driven Pattern in Thin Bilayer Films: Spinodal Wrinkling. *Phys. Rev. Lett.* **2003**, *91*, 1545021−1545024.
(44) David, M. O.; Reiter, G.; Sitthaï, T.; Schultz, J. Deformation of a Glassy Polymer Film by Long-Range Intermolecular Forces. *Langmuir* **1998**, *14*, 5667−5668.
(45) Yoo, P. J.; Suh, K. Y.; Lee, H. H. Short- and Long-Range Interactions in Thin Films of Polymer Blends in Microchannels. *Macromolecules* **2002**, *35*, 3205−3212.
(46) Yoo, P. J.; Suh, K. Y.; Kang, H.; Lee, H. H. Polymer Elasticity-Driven Wrinkling, and Coarsening in High Temperature Buckling of Metal-Capped Polymer Thin Films. *Phys. Rev. Lett.* **2004**, *93*, 034301−1.
(47) Vogel, H. The Law of the Relationship between Viscosity of Liquids and the Temperature. *Z. Phys. Chem.* **1921**, *22*, 645−646.
(48) Tammann, G.; Hesse, W. Die Abhängigkeit der Viscosität von der Temperatur bie Unterkühlten Flüssigkeiten. *Z. Anorg. Allg. Chem.* **1926**, *156*, 245−257.
(49) Fulcher, G. S. Analysis of Recent Measurements of the Viscosity of Glasses.-II. *J. Am. Ceram. Soc.* **1925**, *8*, 789−794.
(50) Chaurasia, S. K.; Singh, R. K.; Chandra, S. Ionic Liquid Assisted Modification in Ionic Conductivity, Phase Transition Temperature and Crystallization Kinetics Behaviour of Polymer Poly(Ethylene Oxide). *Solid State Ionics* **2014**, *262*, 790−794.
(51) Choi, J. W.; Cheruvally, G.; Kim, Y. H.; Kim, J. K.; Manuel, J.; Raghavan, P.; Ahn, J. H.; Kim, K. W.; Ahn, H. J.; Choi, D. S.; Song, C. E. Poly(Ethylene Oxide)-Based Polymer Electrolyte Incorporating Room-Temperature Ionic Liquid for Lithium Batteries. *Solid State Ionics* **2007**, *178*, 1235−1241.
(52) Liu, C.; Ma, X.; Xu, F.; Zheng, L.; Zhang, H.; Feng, W.; Huang, X.; Armand, M.; Nie, J.; Chen, H.; Zhou, Z. Ionic liquid electrolyte of lithium bis(fluorosulfonyl)imide/N-methyl-N-propylpiperidinium bis-(fluorosulfonyl)imide for Li/natural graphite cells: Effect of concentration of lithium salt on the physicochemical and electrochemical properties. *Electrochim. Acta* **2014**, *149*, 370−385.
(53) Matsumoto, H.; Sakaebi, H.; Tatsumi, K. Preparation of Room Temperature Ionic Liquids based on Aliphatic Onium Cations and Asymmetric Amide Anions and their Electrochemical Properties as a Lithium Battery Electrolyte. *J. Power Sources* **2005**, *146*, 45−50.
(54) Lane, G. H. Electrochemical Reduction Mechanisms and Stabilities of Some Cation Types Used in Ionic Liquids and Other Organic Salts. *Electrochim. Acta* **2012**, *83*, 513−528.
(55) Chiappone, A.; Nair, J. R.; Gerbaldi, C.; Jabbour, L.; Bongiovanni, R.; Zeno, E.; Beneventi, D.; Penazzi, N. Microfibrillated Cellulose as Reinforcement for Li-Ion Battery Polymer Electrolytes with Excellent Mechanical Stability. *J. Power Sources* **2011**, *196*, 10280−10288.
(56) Nair, J. R.; Destro, M.; Gerbaldi, C.; Bongiovanni, R.; Penazzi, N. Novel Multiphase Electrode/Electrolyte Composites for Next Generation of Flexible Polymeric Li-Ion Cells. *J. Appl. Electrochem.* **2013**, *43*, 137−145.
(57) Di Lupo, F.; Meligrana, G.; Gerbaldi, C.; Bodoardo, S.; Penazzi, N. Surfactant-Assisted Mild Solvothermal Synthesis of Nanostructured $LiFePO_4$/C Cathodes Evidencing Ultrafast Rate Capability. *Electrochim. Acta* **2015**, *156*, 188−198.
(58) Li, C. T.; Lee, C. P.; Lee, C. T.; Li, S. R.; Sun, S. S.; Ho, K. C. Iodide-Free Ionic Liquid with Dual Redox Couples for Dye-Sensitized Solar Cells with High Open-Circuit Voltage. *ChemSusChem* **2015**, *8*, 1244−1253.
(59) Ng, H. M.; Ramesh, S.; Ramesh, K. Exploration on the P(VP-co-VAc) Copolymer Based Gel Polymer Electrolytes Doped with Quaternary Ammonium Iodide Salt for DSSC Applications: Electrochemical Behaviors and Photovoltaic Performances. *Org. Electron.* **2015**, *22*, 132−139.
(60) Bella, F.; Sacco, A.; Pugliese, D.; Laurenti, M.; Bianco, S. Additives and Salts for Dye-Sensitized Solar Cells Electrolytes: What is the Best Choice? *J. Power Sources* **2014**, *264*, 333−343.
(61) Rong, Y.; Li, X.; Liu, G.; Wang, H.; Ku, Z.; Xu, M.; Liu, L.; Hu, M.; Yang, Y.; Zhang, M.; Liu, T.; Han, H. Monolithic Quasi-Solid-State Dye-Sensitized Solar Cells Based on Iodine-Free Polymer Gel Electrolyte. *J. Power Sources* **2013**, *235*, 243−250.
(62) Lan, Z.; Wu, J.; Wang, D.; Hao, S.; Lin, J.; Huang, Y. Quasi-Solid State Dye-Sensitized Solar Cells Based on Gel Polymer Electrolyte with Poly(Acrylonitrile-co-Styrene)/NaI+I_2. *Sol. Energy* **2006**, *80*, 1483−1488.
(63) Jennings, J. R.; Wang, Q. Influence of Lithium Ion Concentration on Electron Injection, Transport, and Recombination in Dye-Sensitized Solar Cells. *J. Phys. Chem. C* **2010**, *114*, 1715−1724.

DOI: 10.1021/acsami.5b02729
ACS Appl. Mater. Interfaces 2015, 7, 12961−12971